Pergamon

0042-6989(94)00097-2

Vision Res. Vol. 34, No. 23, pp. 3127–3137, 1994

0042-6989/94 $7.00 + 0.00

Temporal Properties of the Red–Green Chromatic Mechanism

RHEA T. ESKEW JR,*† CHARLES F. STROMEYER III,*‡ RICHARD E. KRONAUER*

Received 16 August 1993; in revised form 11 March 1994

The temporal properties of the red–green chromatic mechanism were studied with red and green equiluminant flashes of 1 deg diameter presented in the center of a bright (800–3000 td) yellow adapting field. A subthreshold 200 msec red or green flash makes an immediately subsequent, suprathreshold yellow luminance flash appear tinged with the complementary color. The chromatic flash also makes a subsequent chromatic flash of the same hue harder to detect and identify, and makes a flash of the opposite hue easier to detect and identify. These results indicate that the response of the red–green mechanism changes polarity during its time–course, suggesting that the chromatic temporal impulse–response function has a negative lobe. Pairs of chromatic pulses were used to estimate the shape of the chromatic impulse–response. The estimated impulse–response function has a zero crossing near 90 msec, followed by a long, shallow negative lobe. We also measured threshold-duration functions; the critical duration for the chromatic and luminance flashes is about 95 and 45 msec, respectively. Chromatic sensitivity (measured in cone contrast units) is 10 times greater than luminance sensitivity for long durations, and is 3 times greater for all durations less than 45 msec.

Temporal sensitivity Chromatic impulse–response Equiluminance

INTRODUCTION

Chromatic mechanisms are often characterized as temporally low pass, unlike the bandpass luminance mechanism (Boynton, 1979; Kelly, 1975). However, at moderate to high adaptation levels, sensitivity for red–green flicker declines slightly at frequencies below about 1.5 Hz, suggesting that chromatic mechanisms may be weakly bandpass (Kelly & van Norren, 1977; Swanson, Ueno, Smith & Pokorny, 1987; DePriest, Sclar & Lennie, 1988).

A bandpass mechanism has a multiphasic temporal impulse–response function (IRF), while a low-pass mechanism has a monophasic impulse–response function. Burr and Morrone (1993) and Uchikawa and Ikeda (1986) used a two-pulse technique to estimate the chromatic IRF, and found it to be monophasic. However, their low retinal illuminance ($\sim$200 td) might have reduced inhibition and eliminated the negative lobe. This idea is supported by the results of Swanson *et al.* (1987), who observed that chromatic flicker sensitivity is bandpass at 900 td, but is low-pass below 90 td. Luminance flicker sensitivity also shifts from bandpass to low-pass at low adapting levels (Kelly, 1961). However, Uchikawa and Yoshizawa (1993) recently found evidence for a biphasic chromatic response at 10 td with a two-pulse method.

Detection of a red or green chromatic flash can be facilitated by a coincident, suprathreshold luminance flash, or pedestal (Cole, Stromeyer & Kronauer, 1990; Eskew, Stromeyer, Picotte & Kronauer, 1991). An observation wth the pedestal (Eskew, Stromeyer & Kronauer, 1994) suggests that the chromatic IRF is biphasic. Detection of a 600 msec chromatic flash was facilitated by a 30 msec luminance pedestal presented just after the chromatic onset. The facilitation declined slightly as the luminance flash was delayed further into the chromatic stimulus. A linear mechanism that has a biphasic IRF responds to a chromatic step with a response that rises until the time of the zero-crossing, and thereafter declines as integration is carried into the negative portion of the impulse–response. The chromatic facilitation follows this pattern. In the present study, presenting a chromatic flash (even a subthreshold flash) just prior to the luminance pedestal tinges the pedestal with the opposite hue, suggesting a facilitation of the negative chromatic off-response.

We use moderately high adapting levels. First, we show the existence of the negative lobe of the IRF using the luminance pedestal and a chromatic flash. Next, we measure threshold-duration functions for chromatic and luminance tests. Finally, we estimate the shape of the chromatic IRF with pairs of chromatic pulses.

*Division of Applied Sciences, Harvard University, Cambridge, MA 02138, U.S.A.
†Department of Psychology, 125-NI, Northeastern University, Boston, MA 02115, U.S.A. [*Email* eskew@neu.edu].
‡Department of Psychology, Harvard University, Cambridge, MA 02138, U.S.A.

METHODS

Apparatus

Stimuli were produced with an eight-channel Maxwellian view (Cole *et al.*, 1990). The stimulus consisted of coincident, 1 deg central test disks of red, green and yellow, and matched contiguous annuli (6.2 deg outer diameter), each composed of light from light-emitting diodes (LEDs) passed through interference filters (8–10 nm half-bandwidth). These components were superposed on an intense yellow adapting field of 6.2 deg diameter. Between trials, the stimulus appeared as a uniform yellow disk, since the edge between the test and the surround was not visible. The test area was fixated with the aid of two dark dots separated by 3 deg, placed above and below the test area. The total illuminance was 790–3000 td in different experiments, with the LEDs contributing 250–400 td. The spectral centroid of the filtered red, green, and yellow LEDs was 671, 551 and 579 nm, respectively. The yellow main field metamerically matched the yellow LED and the sum of red and green LEDs.

Stimulus representation

The test LEDs were modulated about their means to produce any desired combination of incremental and decremental flashes. Green chromatic flashes were produced by simultaneous incremental green and decremental red flashes, and red chromatic flashes were produced by inverting the polarities. The luminance pedestal was produced with the yellow LED.

The Smith and Pokorny (1975) cone fundamentals are used to represent the stimuli in the cone contrast coordinates ($\Delta L/L$, $\Delta M/M$). For example, L-cone contrast represents the change in L-cone quantal catch produced by the test flash (ΔL), normalized by the mean L-cone quantal catch (L) owing to all the steady components. The cone contrast metric takes account of the spectral overlap of the L and M cones, and thus threshold differences for luminance and chromatic stimuli reflect differences in post-receptoral mechanisms. In Fig. 4, incremental and decremental luminance flashes are defined as vectors of polar angle 45 and 225 deg, while green and red chromatic flashes are defined as 135 and 315 deg (second and fourth quadrants). Stimulus contrast is specified by the vector length in cone contrast space, $[(\Delta L/L)^2 + (\Delta M/M)^2]^{1/2}$.

Calibration

The mean radiances of the lights were calibrated each session. The test light intensities were modulated by current amplifiers, controlled by 12-bit DACs. The current amplifiers contain low-pass filters to eliminate a small, brief light overshoot at flash onset. These filters slightly elongate the light pulses. The left side of Fig. 1 shows nearly-identical oscilloscopic tracings for nominal 10-msec red and green pulses. The right side shows a rectangular pulse of the same area and peak amplitude as the actual pulse; this equivalent pulse is 11 msec long.

General procedure

Thresholds were measured with a temporal two-alternative forced-choice (2AFC) method, with the two intervals separated by 400 msec. The test color was typically either red or green throughout a run of 150–200 trials. Tones signaled the intervals and provided response feedback, except in the first experiment where there was no feedback.

For each threshold estimate, frequency-of-seeing data were obtained with two or more Quest staircases (Watson & Pelli, 1983) randomly interleaved in a run. On each trial, the test amplitude was the current estimate of the 82%-correct point, with a random jitter of ± 0.1 log units. The frequency-of-seeing data for a single test condition (400–800 trials) were fitted by the Weibull function, using a maximum likelihood criterion:

$$P(a) = 1 - \tfrac{1}{2} \cdot \exp[-(a/\hat{a})^{\beta}] \quad (1)$$

where $P(a)$ is the probability of a correct response for a stimulus of contrast a, $\frac{1}{2}$ is the probability of a correct response by chance, $\hat{a}$ (the threshold) is the value of a for 82% correct, and β is the slope parameter. A 90% χ^2 confidence interval was calculated for the fit.

Thresholds were also measured for chromatic identification. A red or green chromatic flash was presented on a trial and the observer made a relative judgment, choosing, for example, the *redder*-appearing interval—the interval containing the red test when it was presented, and the interval *not* containing the test flash (the blank interval) when the green test was presented (Cole *et al.*, 1990). Without requiring the observer to make a relative judgment of this sort, adaptive procedures like Quest can be severely affected by response bias.

RESULTS

The negative chromatic lobe

We first show that the response to a weak chromatic flash reverses sign over time, indicating that the chromatic IRF has a negative lobe.

We used a luminance pedestal to facilitate any opposite-colored rebound at the end of the chromatic flash. A 200 msec luminance flash of 2× threshold was presented in both trial intervals. Presented alone, the luminance pedestal appeared yellow—the same hue as

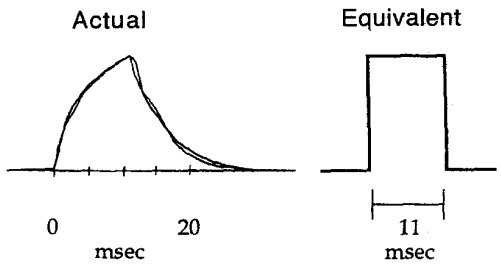

FIGURE 1. Two oscilloscope tracings (left), of red and green LED nominal square light pulses of 10 msec. The 11 msec rectangular pulse on the right has the same peak and integral as the pulse on the left.

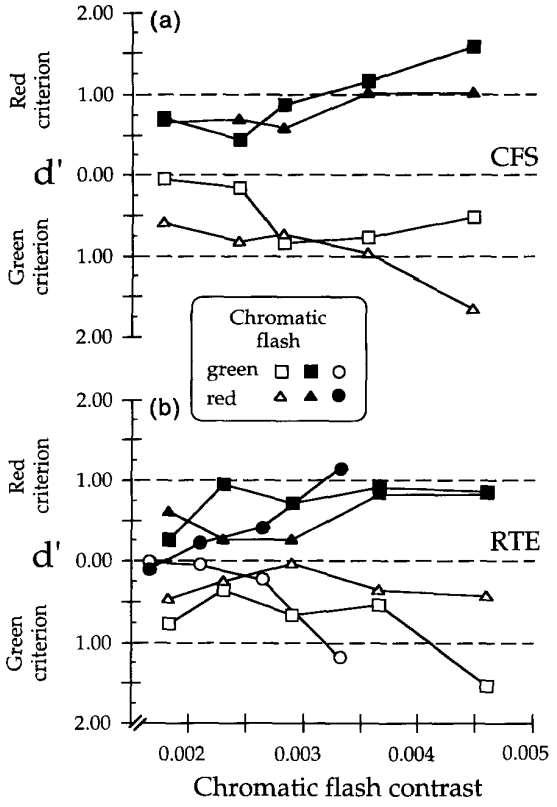

FIGURE 2. Chromatic identification thresholds, expressed as d'. The squares and triangles represent judgments of the hue induced into an achromatic pedestal by a weak chromatic flash (of the contrast specified by the abcissa) immediately preceding the pedestal. Squares are for a green flash, triangles for a red one. Observers selected either the greener- or redder-appearing pedestal, in different runs. The weak chromatic flash made the pedestal appear tinged with the opposite hue (see text). Circles (b) are for standard chromatic identification of the chromatic flash itself. The adapting field was 3000 td.

the field. In one randomly selected interval of each trial, the luminance pedestal was immediately preceded by either a 200 msec red or green chromatic flash. If there is a chromatic off-response it may tinge the pedestal with the hue opposite to the chromatic flash.

Figure 2 plots d' for chromatic identification as a function of the contrast of the chromatic flash. The task was to judge the relative hue of the two luminance pedestals in each trial. In separate runs the observer was instructed to choose either the redder-appearing pedestal (red criterion) or greener-appearing pedestal (green criterion). First consider the squares, which show results for trials where the chromatic flash was *green*. The response was scored correct when the observer selected the interval containing the green chromatic flash. As the green flash contrast is raised, d' rises when the observer is told to choose the red-appearing pedestal (red criterion, solid squares). Using exactly the same stimuli, d' also rose when we switched to the opposite green criterion (open squares), but this is because we also switched the scoring rule so the interval *not* containing the green chromatic flash was judged correct. Thus for both criteria, the green chromatic flash makes the pedestal appear redder. An analogous treatment of the results of trials with the red chromatic flash shows that red flashes make the pedestal appear green.

For the squares and triangles, the observer ignored the chromatic flash if it was seen, attempting to judge the hue of the pedestal. The circles in Fig. 2(a) show chromatic identification thresholds for the chromatic flashes themselves measured with the *same* stimulus conditions (the pedestal was present). Flashes that are themselves very poorly visible (flashes near 0.002, for which $d' \cong 0$) nevertheless affect the color of the pedestal (squares and triangles). The pedestal may act to mask the on response to the chromatic flash (Eskew *et al.*, 1994), while facilitating its off-response.

We next measured the effect of the chromatic flash on a second chromatic flash (200 msec) presented immediately after the first flash. The first, or conditioning, flash was presented in both trial intervals, and was immediately followed in one interval by the second flash, the test

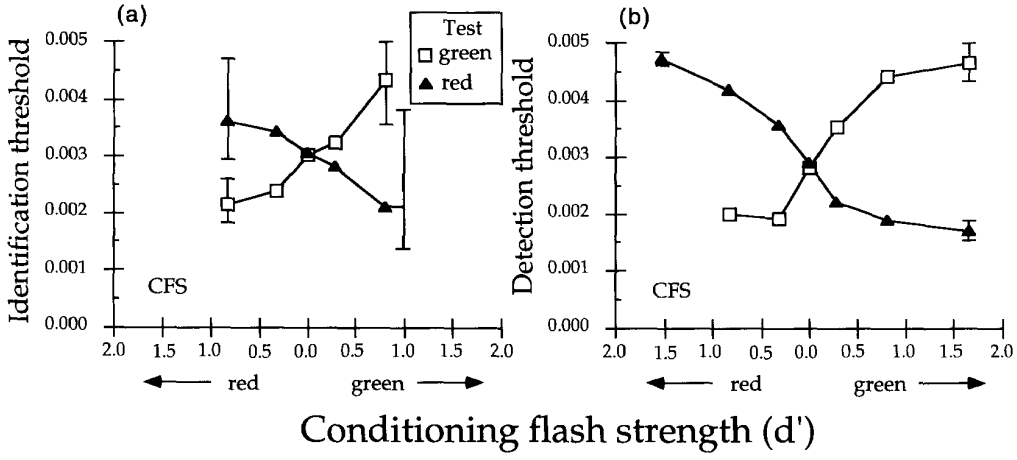

FIGURE 3. Chromatic identification (a) and detection (b) of a 200 msec red or green chromatic test flash, as a function of the contrast and color (red or green) of the immediately preceding 200 msec conditioning flash (abscissa). Only the confidence interval around the left- and right-most points are drawn (the interval was smaller than the symbol in one case). The adapting field was 3000 td.

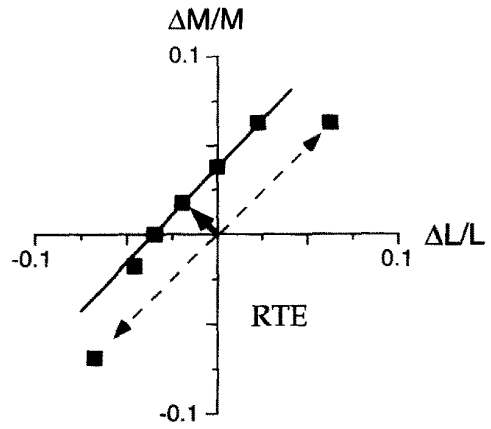

FIGURE 4. Detection thresholds for 11 msec flashes, plotted in ($\Delta L/L$, $\Delta M/M$) coordinates. Luminance thresholds are plotted at 45 and 225 deg (dashed arrows); chromatic thresholds are fit with a straight line. The approximately-equiluminant green test direction used in the other experiments is indicated by the solid arrow. The adapting field was 990 td.

flash. Figure 3 shows chromatic identification thresholds [Fig. 3(a)] and detection thresholds [Fig. 3(b)] for the test flash as a function of the color and contrast of the prior conditioning flash. The conditioning flash strength is represented in d' units, indicating its visibility (measured separately). The test flash is harder to detect and identify when preceded by a same-colored conditioning flash, but both tasks are facilitated by an opposite-colored conditioning flash. Even very weak conditioning flashes are effective. Using incremental monochromatic flashes rather than the approximately-equiluminant flashes used here, Stromeyer, Khoo, Muggeridge and Young (1978) observed a similar facilitation effect with a sequential green–red pair of lights.

This first series of experiments indicate that the response to a 200-msec chromatic flash changes polarity over its time-course. This tinges the luminance pedestal with opposite hue and facilitates a subsequent chromatic flash that is opposite in hue to the first flash. Linearity ought to hold for these weak stimuli, and thus the change in chromatic polarity indicates that the chromatic IRF has a negative lobe.

Evidence for chromatic detection of 11 msec pulses

Short pulses will be used to measure the chromatic IRF. First we show that these brief pulses are detected by the red–green mechanism, by measuring a detection contour and threshold-duration functions.

The detection contour in Fig. 4 shows thresholds for 11 msec flashes (Fig. 1) that modulate the L and M cones in different ratios. The fitted straight line has a slope near unity (1.06), indicating detection by a mechanism that responds to $\Delta M/M - \Delta L/L$. The luminance thresholds at 45 and 225 deg are about 3 times higher than the chromatic threshold at 135 deg (dashed vs solid arrows), showing that the chromatic mechanism is more sensitive than the luminance mechanism for very brief flashes (Stromeyer, Cole & Kronauer, 1985; Chaparro, Stromeyer, Huang, Kronauer & Eskew, 1993).

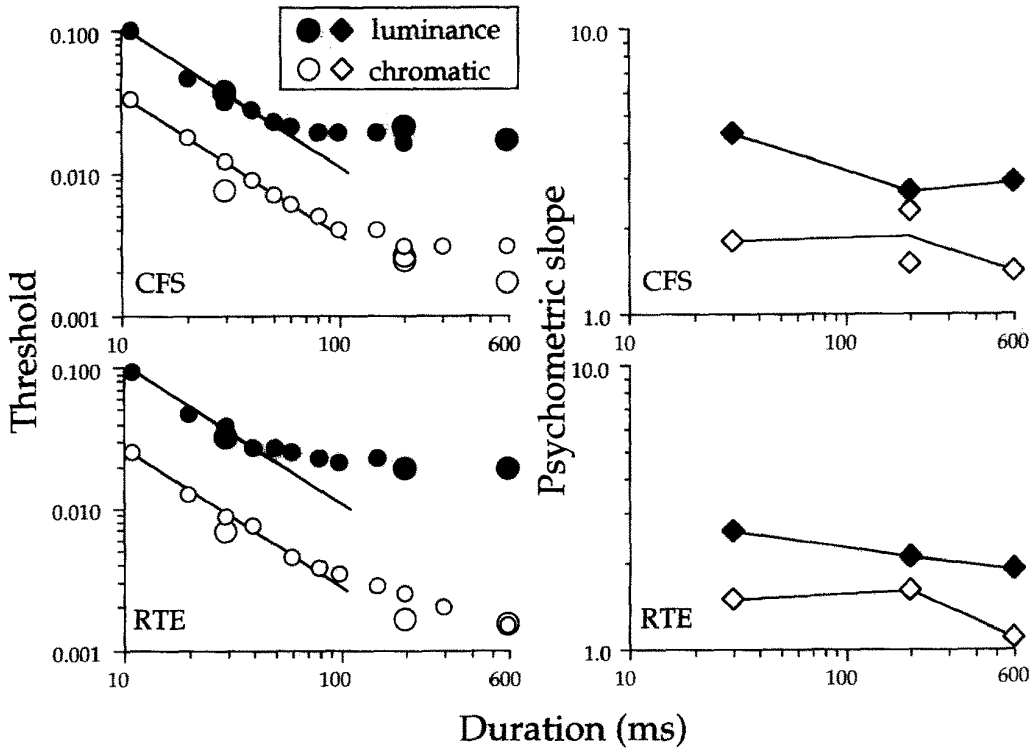

FIGURE 5. Thresholds (left) and psychometric slopes, β (right), for positive luminance flashes and green chromatic flashes as a function of duration. For the smaller symbols, the adapting field was 1150 td. Larger symbols (including all of the β values) were measured using the method of constant stimuli, with a 3000 td adapting field.

The left panel of Fig. 5 shows luminance and chromatic thresholds as a function of duration. The straight lines, of slope −1, show that Bloch's law critical duration is 40–50 msec for the luminance flash, and 90–100 msec for the chromatic flash, confirming the well-known longer integration for chromatic signals (Regan & Tyler, 1971a; Schwartz & Loop, 1984; Smith, Bowen & Pokorny, 1984). For long flashes, the chromatic mechanism is ~10× more sensitive than the luminance mechanism, and this ratio drops to 3× for flashes less than 40 msec. This chromatic advantage will obtain at all shorter durations, assuming Bloch's law. The higher cone contrast sensitivity for chromatic flashes could reflect greater spatial summation for chromatic stimuli or lower gain in the luminance channel; we found a similar chromatic advantage when thresholds are analyzed in cone contrast energy units (Chaparro *et al.*, 1993), which are unaffected by spatial integration differences.

The right panel in Fig. 5 shows the psychometric function slope, β, measured with the method of constant stimuli, for luminance and chromatic flashes of three durations. The slopes are steeper for luminance than chromatic flashes (Cole *et al.*, 1990; Stromeyer, Lee & Eskew, 1992), and the slopes tend to decrease with duration, perhaps reflecting lower detection uncertainty at longer durations (Lasley & Cohn, 1991).

Two-pulse measurements

Pairs of 11 msec chromatic pulses were used to measure the chromatic IRF. The two pulses were separated by an interstimulus interval (ISI) of δ msec; the contrast of the first and second pulses is a_0 and a_1. Green and red pulses are denoted by, respectively, positive and negative values of a; the figures show the absolute value of the contrast of the second pulse, a_1. The task was to detect the pulse pair, presented in one of the trial intervals; the other trial interval was blank. Two procedures were used to determine threshold: either a_0 was fixed at a low contrast and a_1 was varied, or the contrast of both pulses was varied together, with $|a_0| = |a_1|$.

Fixed first pulse. The contrast of the first pulse, a_0, was fixed, and the contrast of the second pulse, a_1, was varied. When the contrast of the second pulse is very low, the detection probability for the pulse pair approaches the detection probability for the first pulse alone [cf. equation (1)]

$$P(a_0) = 1 - [1 - \tfrac{1}{2}] \cdot \exp[-(a_0/\hat{a})^{\beta}] = \text{constant}. \quad (2)$$

$P(a_0)$ was estimated from data for a single red or green pulse measured over several months; Table 1 (middle) shows the contrast of the first pulse, a_0, and its detection probability, $P(a_0)$.

The detection probability of the pulse pair is given by

$$P_{\delta}(a_1|a_0) = 1 - [1 - P(a_0)] \cdot \exp[-(a_1/\hat{a}_{\delta})^{\beta_{\delta}}] \quad (3)$$

where δ is the ISI between the two pulses. Equation (3) may be regarded simply as a means of fitting the measured frequency-of-seeing data to estimate the 82% detection point. Although equation (3) is written in the form of a probability sum of independent detection of the two pulses, the two pulses are not detected independently at small ISIs. The responses to the two pulses will interact deterministically and thus affect the estimated values of β_{δ} and $\hat{a}_{\delta}$; this deterministic interaction is what we wish to measure (if the two pulses are independent except for probability summation, and if the high threshold assumption holds, then the thresholds $\hat{a}_{\delta}$ would all be equal to $\hat{a}$, the threshold for a single pulse alone). Owing to the difficulty in estimating β (Maloney,

TABLE 1

Observer	Mean threshold for single 11 msec flash		
RTE	0.028 (0.004)		
CFS	0.036 (0.002)		
	First flash color	$\lvert a_0 \rvert$	$P(a_0)$
First two-pulse experiment			
RTE	Red	0.011	0.59
	Green	0.011	0.59
CFS	Red	0.011	0.53
	Green	0.011	0.53
Second two-pulse experiment			
RTE	Red	0.020	0.67
	Green	0.020	0.75
CFS	Red	0.024	0.65
	Green	0.024	0.66

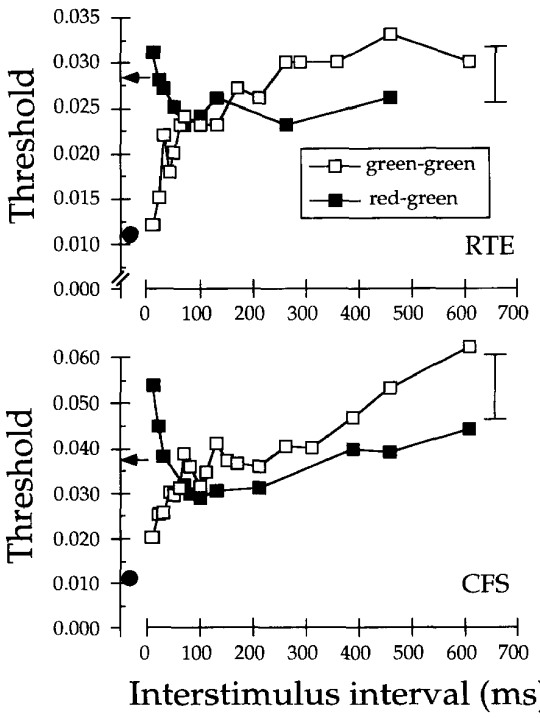

FIGURE 6. Detection thresholds ($|\hat{a}_1|$) as a function of the ISI between two 11 msec chromatic pulses. The legend indicates the pulse colors. Different ordinate scales are used for the two observers to better reveal the time-varying features of the data. The bar at the right depicts the average 90% confidence interval. The arrow indicates the average threshold for a single 11-msec pulse, and the solid circle shows the intensity of the first, fixed pulse ($|a_0|$). The adapting level was 1200 td (RTE) and 1150 td (CFS).

1990), the results are based only on the threshold parameter, $\hat{a}_\delta$, with each observer's average slope value used for β.

Figure 6 shows thresholds for both green–green and red–green pulse pairs. A single ISI was used in each run. The threshold $\hat{a}_\delta$ at each ISI was estimated with equation (3). At small ISIs, the threshold for the green–green pair is lower than the red–green pair, but this relationship reverses at longer ISIs—at about 90–125 msec for RTE, and 50–100 msec for CFS. The reversal reveals a negative lobe of the IRF. However, the effect is small. The vertical bar at the right indicates the average 90% χ^2 confidence interval of single threshold estimates.

Thresholds for observer CFS tend to generally rise at long ISIs, where there is a long delay between the warning tone signal and the second pulse. The threshold rise could be caused by eye movements or temporal uncertainty. To control for this, we next presented the second (test) pulse always 450 msec after the warning tone (the interval between the warning signal and the weak first pulse was varied). Five ISIs were intermixed within a run. The intensity of the first pulse, a_0, was again fixed, and the pulse polarity was constant in each run. The contrast and detectability of the first pulse are given in Table 1 (bottom).

Threshold contrasts of the second (test) pulse $|\hat{a}_1|$ are shown in Fig. 7; open symbols indicate pulse pairs of the same color and solid symbols indicate opposite colors. In the left panels the test pulse was green, and in the right panels it was red. In three of the four cases, the two functions appear to cross, although again the effect is small relative to the average confidence interval (shown at right). CFS's thresholds tend to be higher in Fig. 7 than Fig. 6; this could be a result of intermixing the ISIs.

To better show the crossover, the difference between the two functions in each panel of Figs 6 and 7 is shown in Fig. 8. Use of this heterochromatic-homochromatic difference helps control for small changes in baseline sensitivity across ISIs. For CFS, the crossover occurs at an ISI of 60 msec, while it does not occur until 90 msec for RTE.

Variable first pulse. In the previous two experiments, the contrast of the first pulse was fixed and that of the second was varied. We next equate the pulse contrasts $|a_0| = |a_1|$, and then simultaneously vary the contrasts together to find threshold. This procedure (with the two pulses in a fixed ratio) is frequently used in luminance two-pulse experiments (Rashbass, 1970; Watson, 1986), and was used by Burr and Morrone (1993) and Uchikawa and Yoshizawa (1993) with chromatic pulses. The experiment was like the last one in terms of timing and intermixing the ISIs. The first pulse was green or red, and the second was green.

Thresholds (Fig. 9, left panels) were derived by fitting equation (1) to the frequency-of-seeing data. For RTE, the two threshold functions apparently cross at about 75 msec, although the effect is quite small; for CFS there is no clear crossover. The hetero-homochromatic difference is plotted on the right. The larger symbols on the right show a replication at a slightly lower adapting level (790 td), with heterochromatic and homochromatic pulse pairs intermixed within a run. These data show

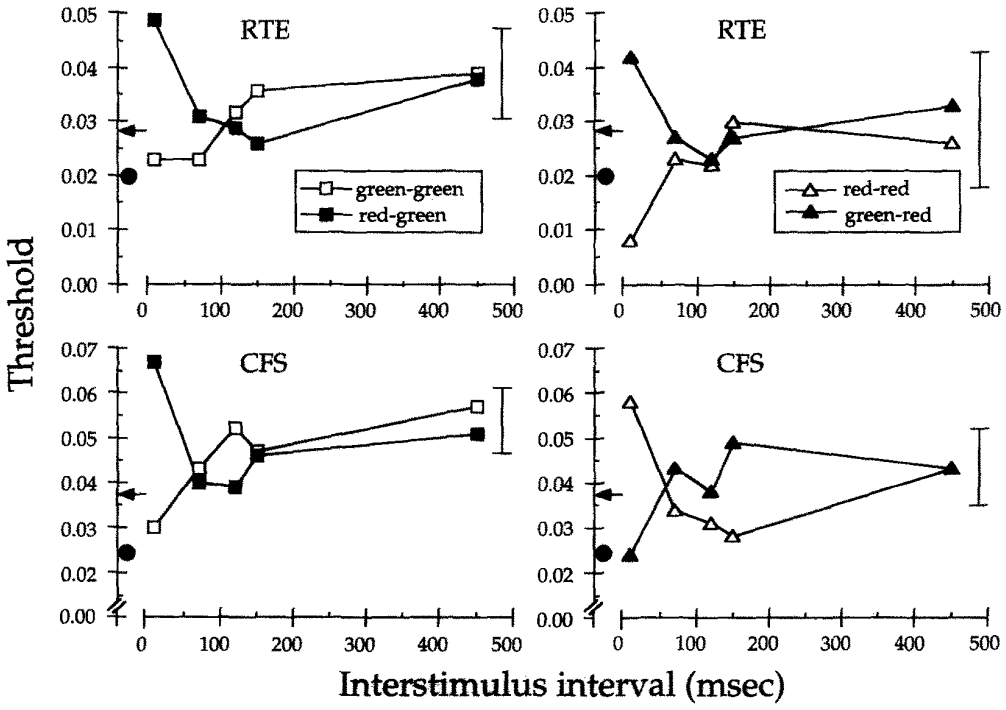

FIGURE 7. Detection thresholds ($|\hat{a}_1|$) as a function of the interval between two 11 msec chromatic pulses. The second pulse was green in the left panels, and red in the right ones. The second pulse occurred 450 msec into the 2AFC interval, and the five ISIs for each curve were intermixed in single runs. Arrows and solid circles as in Fig. 6. The adapting level was 1200 td (RTE) and 830 td (CFS).

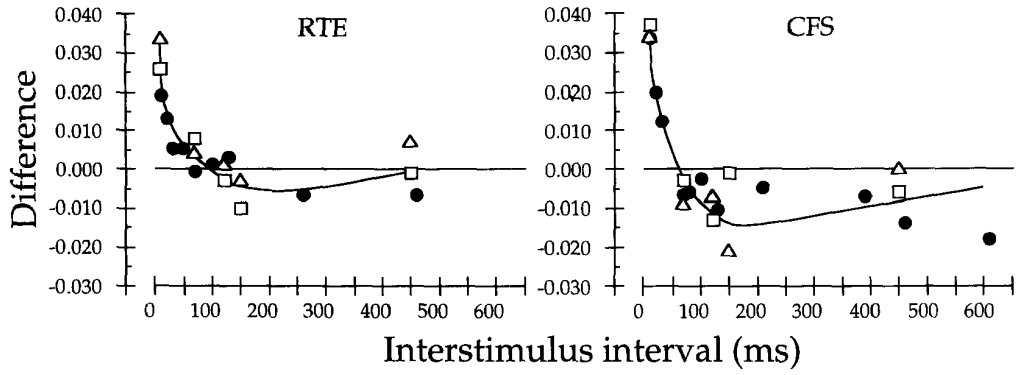

FIGURE 8. Threshold difference between heterochromatic and homochromatic flash pairs as a function of ISI. Circles are from Fig. 6, and squares and triangles are from Fig. 7 (open squares and solid circles are for a green second pulse, open triangles for a red one). The curves are drawn by eye near the averages of the points. The curves approximate the shape of the IRF assuming a peak detector.

that the crossover, although weak, appears to be replicable. Note the different depths of the negative values in Figs 8 and 9. As discussed later, the most likely reason for this difference is that the present experiment, $|a_0|$ is generally larger than in the previous experiments. The observer might often base his judgment on the large first pulse in the present experiment, and thus less crossover might be observed.

DISCUSSION

The response to a 200 msec chromatic flash changes polarity during its time–course. A very weak red or green flash causes a subsequent luminance pedestal to appear tinged with the opposite color. The chromatic flash also makes a subsequent chromatic flash of the same color harder to detect and identify, and makes a subsequent

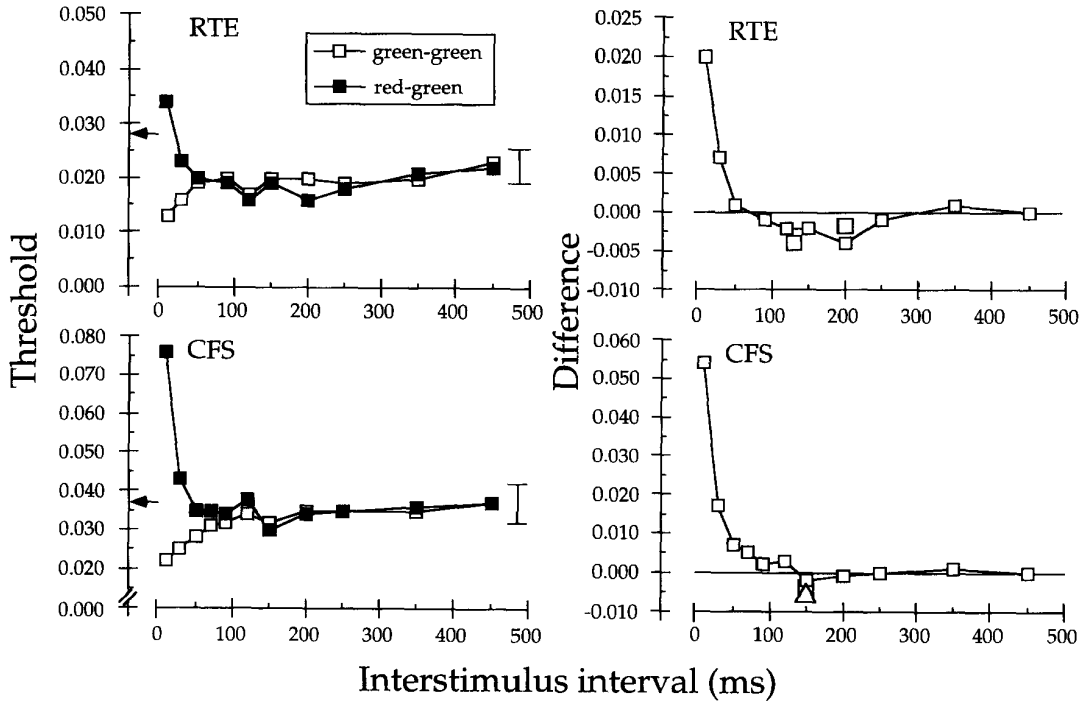

FIGURE 9. Left panels: detection thresholds for pulse pairs (red–green or green–green) as a function of ISI. The threshold contrast is plotted as $|\hat{a}_0|$ or $|\hat{a}_1|$, since the two members of each pair were equated in contrast. The arrow indicates the threshold of a single pulse. The adapting level was 990 td. Right panels: difference between the two functions plotted on the left. Larger symbols indicate replications at 790 td: squares are for a green second pulse, triangles for a red second pulse. In the bottom right panel three symbols coincide at 150 msec. Even assuming peak detection, the curves on the right do not approximate the shape of the IRF.

chromatic flash of the opposite color easier to detect and identify.

This change of polarity was confirmed with pairs of 11 msec chromatic pulses, especially when the first pulse was weak and fixed in intensity.

Modeling the impulse–response function

Let $y(t)$ represent the response to the equiluminant stimulus $x(t)$. Then for weak stimuli for which we may assume linearity

$$y(t) = \int_0^\infty h(\tau)x(t-\tau)\,d\tau.$$

In our experiments $x(t)$ consists of two 11 msec pulses separated by δ msec. We denote the response to this stimulus by $y_\delta(t)$. We assume that the 11 msec pulse is brief enough to serve as a true impulse, and so the response to two impulses is simply

$$y_\delta(t) = a_0 h(t) + a_1 h(t-\delta) \tag{4}$$

where h is the IRF we wish to estimate.

The IRF can be modeled as the difference of two n-stage filters. Responses based on the initial rising portion of the IRF could not be measured (see Appendix). The initial rise was estimated by fitting the model to the entire set of data; this estimate depends critically on the number of stages assumed for the first filter. The first filter has the shorter time constant and is primarily responsible for the steep rise in the IRF and for the sensitivity to high-frequency flicker. The number of stages in the first filter can be estimated from the fall-off in chromatic sensitivity at high flicker rates. Wisowaty (1981) observed a high-frequency slope in log–log coordinates of about -2 to -4. Stromeyer, Cole and Kronauer (1987) found a slope of between -2 and -3 for their data and for replotted data of Varner, Jameson and Hurvich (1984). The results likely underestimate the asymptotic slope, so five stages were assumed for the first filter.

The number of stages in the second filter is more difficult to estimate. Assuming five stages would lead to difficulty in fitting the data, given the rather steep derivatives near the apparent zero-crossing (Fig. 8). Based upon preliminary calculations, the second filter was assumed to have two stages.

The detection process

The derivation of the IRF depends upon the detection process (Watson, 1982). We consider both peak detection (Swanson *et al.*, 1987) and probability summation over time (Watson, 1979). Both models contain an early filtering stage, followed by a later decision stage. A peak detector responds when the internal signal reaches threshold, whereas the probability summation model assumes information is accumulated stochastically over the stimulus interval.

The most informative data for choosing the decision process are the thresholds for pulse pairs at long ISIs and thresholds for flashes of long durations, since for these data the choice of decision process has a much larger effect on the model fit than does reasonable variation in the filter parameters. Unfortunately, different parts of our data are consistent with each decision processes. (1) Probability summation is suggested by the continuing decline in threshold for flashes longer than Bloch's critical time (Fig. 5), with a slope near $-1/\beta$ (Watson, 1986). (2) Probability summation implies that the threshold for pairs of pulses at large ISIs should be lower than the threshold for a single pulse (given by the arrow in Figs 6, 7 and 9), and this should be independent of the polarities of the pair. Figure 9 shows this pattern, but Figs 6 and 7 generally do not.

The data thus do not strongly support one decision process over the other. We will assume a peak detector owing to its simplicity; however, our major conclusions would be similar had we chosen the probability summation model (see Appendix).

Fitted impulse–response functions

The impulse–response is characterized (Watson, 1986),

$$h(t) = M\{f_1(t) - Tf_2(t)\} \tag{5}$$

where each f represents an n-stage linear filter

$$f(t) = [\tau(n-1)!]^{-1}\cdot[(t/\tau)^{n-1}]\cdot\exp(-t/\tau). \tag{6}$$

The two filters are normalized to have unit area. The model was simultaneously fit to the data of Figs 6, 7, and 9 by minimizing the sum of

$$[\max\{|y_\delta(t)|\} - 1]^2$$

with $y_\delta(t)$ defined by equations 4–6. The derived IRFs are shown in Fig. 10, with parameters specified in Table 2. The transience parameter, T [equation (5)], determines the relative areas of the positive and negative lobes of the IRF. The best value of T for both observers was >1.0; however, T was set to 1.0 so that the IRF would not integrate to a negative value at very long times. Constraining T trivially increases the residual of the fit, leaves the zero-crossing almost unchanged, but does reduce the estimated time constant of the second filter by 30–50 msec. (Most of the effect of allowing $T > 1.0$ occurs at long ISIs where we have little data.) The negative lobe is shallow, but the fits are substantially worse when T is set to zero or if the second lobe is made positive.

The proportion of variance accounted for is specified by r^2 (Table 2). The derived IRFs provide a good fit to the two-pulse data of CFS and an adequate fit to the data of RTE. The initial portions of the IRFs are similar for the two observers; however, CFS has a slightly earlier zero crossing. The IRFs tend to underestimate ($\sim 5\%$) the extreme thresholds, as indicated by a plot (not shown) of actual vs predicted $\hat{a}_1$.

Our IRFs, based upon 1 deg test spots, are rather different in shape from the 0.5 or 2 deg chromatic IRFs of Swanson *et al.* (1987) obtained at 900 td, although their IRFs did have a negative lobe. They used a model with three filters rather than two, with pure delays between the filters. These extra parameters might have

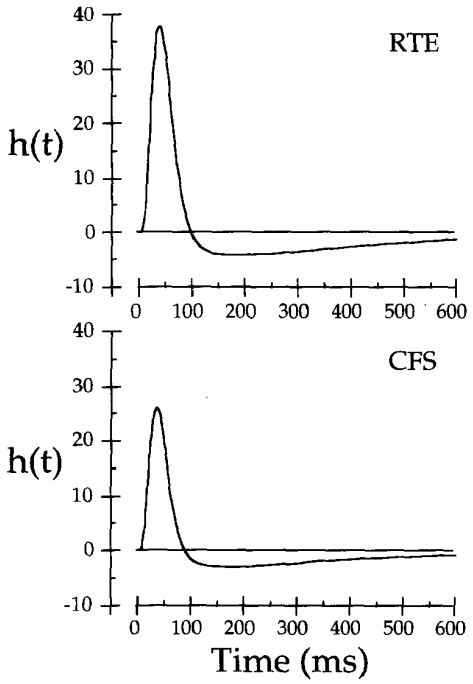

FIGURE 10. Estimated impulse response functions $h(t)$ (in sec^{-1}) for the two observers. Data from Figs 7 and 9 were weighted double relative to Fig. 6. Parameters are specified in Table 2.

improved the fits of our IRFs but could reduce the generality of the model.

The modulus of the Fourier transform of these IRFs (not shown) has a small decline below 1 Hz, consistent with the chromatic flicker data of Kelly and van Norren (1977), Swanson *et al.* (1987) and Regan and Tyler (1971b, Fig. 1b—no-surround condition).

The peak detector model provides a summary of the two-pulse data. However, the probability summation model may be more correct than the peak detector model at threshold (Georgeson, 1987; Nachmias, 1981). For instance, the peak detector predicts a threshold-vs-duration function with slope of -1 at short duration and slope of zero at longer durations, which would provide a very poor fit to our data (Fig. 5). The most realistic model is likely to include probability summation over a restricted, and perhaps variable, time period (Gorea & Tyler, 1986). The current data put few constraints on this time, so we adopted the peak detector for simplicity. The limited integration time of the detection stage is the most plausible explanation of the reduced crossover shown in Fig. 9. In Fig. 9 the first pulse was of higher contrast than in Figs 6 and 7; to the extent that the observer could respond to the first pulse alone, the two pulses would not interact and little crossover would be observed. This reasoning suggests that two-pulse experiments that keep $|a_0| = |a_1|$, such as those of Uchikawa and Yoshizawa (1993) and Burr and Morrone (1993), may underestimate the duration of the IRF, and perhaps miss a second lobe.

TABLE 2. Fitted IRF parameter values

	RTE	CFS
M	2.008	1.243
T	1.00	1.00
First filter		
n	5	5
τ (msec)	9.8	8.8
Second filter		
n	2	2
τ (msec)	176	158
r^2	0.71	0.91

The negative lobe in the estimated chromatic IRF is quite shallow, compared to estimates of the negative lobe of the luminance IRF (Watson, 1986). However, the negative lobe is deep enough to produce such effects as a decline in sensitivity during a chromatic flash (Eskew *et al.*, 1994) and the chromatic offset rebound, since these effects depend upon integrating the IRF.

REFERENCES

Boynton, R. M. (1979). *Human color vision*. New York: Holt (Rinehart & Winston).

Burr, D. C. & Morrone, M. C. (1993). Impulse-response functions for chromatic and achromatic stimuli. *Journal of the Optical Society of America A, 10*, 1706–1713.

Chaparro, A., Stromeyer, C. F. III, Huang, E. P., Kronauer, R. E. & Eskew, R. T. Jr (1993). Colour is what the eye sees best. *Nature, 361*, 348–350.

Cole, G. R., Stromeyer, C. F. III & Kronauer, R. E. (1990). Visual interactions with luminance and chromatic stimuli. *Journal of the Optical Society of America A, 7*, 128–140.

DePriest, D. D., Sclar, G. & Lennie, P. (1988). Central limits to chromatic flicker-sensitivity. *Investigative Ophthalmology and Visual Science (Suppl.), 29*, 326.

Eskew, R. T. Jr, Stromeyer, C. F. III & Kronauer, R. E. (1994). The time-course of chromatic facilitation by luminance contours. *Vision Research, 34*, 3139–3144.

Eskew, R. T. Jr, Stromeyer, C. F. III, Picotte, C. J. & Kronauer, R. E. (1991). Detection uncertainty and the facilitation of chromatic detection by luminance contours. *Journal of the Optical Society of America A, 8*, 394–403.

Georgeson, M. A. (1987). Temporal properties of spatial contrast vision. *Vision Research, 27*, 765–780.

Gorea, A. & Tyler, C. W. (1986). New look at Bloch's law for contrast. *Journal of the Optical Society of America A, 3*, 52–61.

Kelly, D. H. (1961). Visual responses to time-dependent stimuli. I. Amplitude sensitivity measurements. *Journal of the Optical Society of America, 51*, 422–429.

Kelly, D. H. (1975). Luminous and chromatic flickering patterns have opposite effects. *Science, 188*, 371–372.

Kelly, D. H. & van Norren, D. (1977). Two-band model of heterochromatic flicker. *Journal of the Optical Society of America, 67*, 1081–1091.

Lasley, D. J. & Cohn, T. E. (1991). Stimulus duration can modify stimulus uncertainty. *Investigative Ophthalmology and Visual Science (Suppl.), 32*, 842.

Maloney, L. T. (1990). Confidence intervals for the parameters of psychometric functions. *Perception & Psychophysics, 47*, 127–134.

Nachmias, J. (1981). On the psychometric function for contrast detection. *Vision Research, 21*, 215–223.

Press, W. H., Flannery, B. P., Teukolsky, S. A. & Vetterling, W. T. (1986). *Numerical recipess: The art of scientific computing*. Cambridge: Cambridge University Press.

Rashbass, C. (1970). The visibility of transient changes of luminance. *Journal of Physiology, London, 210*, 165–186.

Regan, D. & Tyler, C. W. (1971a). Temporal summation and its limit for wavelength changes: An analog of Bloch's law for color vision. *Journal of the Optical Society of America A, 61*, 1414–1421.

Regan, D. & Tyler, C. W. (1971b). Some dynamic features of colour vision. *Vision Research, 11*, 1307–1324.

Roufs, J. A. J. & Blommaert, F. J. J. (1981). Temporal impulse and step responses of the human eye obtained psychophysically by means of a drift-correcting pertubation technique. *Vision Research, 21*, 1203–1221.

Schwartz, S. H. & Loop, M. S. (1984). Effect of duration on detection by the chromatic and achromatic systems. *Perception & Psychophysics, 36*, 65–67.

Smith, V. C. & Pokorny, J. (1975). Spectral sensitivity of the foveal cone photopigments between 400 and 500 nm. *Vision Research, 15*, 161–171.

Smith, V. C., Bowen, R. W. & Pokorny, J. (1984). Threshold temporal integration of chromatic stimuli. *Vision Research, 24*, 653–660.

Stromeyer, C. F. III, Cole, G. R. & Kronauer, R. E. (1985). Second-site adaptation in the red–green chromatic pathways. *Vision Research, 25*, 219–237.

Stromeyer, C. F. III, Cole, G. R. & Kronauer, R. E. (1987). Chromatic suppression of cone inputs to the luminance flicker mechanism. *Vision Research, 27*, 1113–1137.

Stromeyer, C. F. III, Lee, J. & Eskew, R. T. Jr (1992). Peripheral chromatic sensitivity for flashes: A post-receptoral red–green asymmetry. *Vision Research, 32*, 1865–1873.

Stromeyer, C. F. III, Khoo, M. C. K., Muggeridge, D. & Young, R. A. (1978). Detection of red and green flashes: Evidence for cancellation and facilitation. *Sensory Processes, 2*, 248–271.

Swanson, W. H., Ueno, T., Smith, V. C. & Pokorny, J. (1987). Temporal modulation sensitivity and pulse-detection thresholds for chromatic and luminance perturbations. *Journal of the Optical Society of America A, 4*, 1992–2005.

Uchikawa, K. & Ikeda, M. (1986). Temporal integration of chromatic double pulses for detection of equal-luminance wavelength changes. *Journal of the Optical Society of America A, 3*, 2109–2115.

Uchikawa, K. & Yoshizawa, T. (1993). Temporal responses to chromatic and achromatic change inferred from temporal double-pulse integration. *Journal of the Optical Society of America A, 10*, 1697–1705.

Varner, D., Jameson, D. & Hurvich, L. M. (1984). Temporal sensitivities related to color theory. *Journal of the Optical Society of America A, 1*, 474–481.

Watson, A. B. (1979). Probability summation over time. *Vision Research, 19*, 515–522.

Watson, A. B. (1982). Derivation of the impulse response: Comments on the method of Roufs and Blommaert. *Vision Research, 22*, 1335–1337.

Watson, A. B. (1986). Temporal sensitivity. In Boff, K. R., Kaufman, L. & Thomas, J. P. (Eds), *Handbook of perception and human performance. Vol. I. Sensory processes and perception*. New York: Wiley.

Watson, A. B. & Pelli, D. G. (1983). QUEST: A Bayesian adaptive psychometric method. *Perception & Psychophysics, 33*, 113–120.

Wisowaty, J. J. (1981). Estimates for the temporal response characteristics of chromatic pathways. *Journal of the Optical Society of America, 71*, 970–977.

Acknowledgements—Research supported by NIH EY-01808, NIH EY-09712, AFOSR 86-0338 and AFOSR 89-0304. We are grateful for advice from Drs Vivianne Smith, Adam Reeves and Richard Humanski.

APPENDIX

This Appendix compares the peak detector model with the probability summation model (Watson, 1979). The latter is typically applied in situations in which the contrast of the test can be factored out of the response expression, such as when the stimulus consists of two equal-amplitude pulses and $y(t) = a_0 h(t) + a_1 h(t-\delta) = a[h(t) + h(t-\delta)]$, equation (4). Here we discuss some limitations of two-pulse experiments in general, and derive a method for applying the probability summation model when one pulse has a fixed amplitude and the other varies, as in the first two of our two-pulse experiments.

The peak detector responds whenever

$$\max\{|y_\delta(t)|\} > 1.0, \tag{A1}$$

where δ is the ISI.

For the probability summation model, the probability P of detection is

$$P(a|\delta) = 1 - \exp\left[-\int_0^\infty |y_\delta(t)|^\beta \, dt\right]. \tag{A2}$$

Inferences from two-pulse data

We denote the measured two-pulse threshold as a function of ISI by $\hat{a} = F[\delta] + F[\infty]$; $\hat{a}$ is chosen to give 82% correct detection, and $F[\infty]$ is the threshold when the two pulses are separated by an ISI greater than the duration of the IRF. In Figs 8 and 9, we plot the heterochromatic-homochromatic difference, as a way of averaging the thresholds and eliminating polarity-independent trends (see discussion of Fig. 7). Denote the heterochromatic and homochromatic data by $F_-[\delta] + F[\infty]$ and $F_+[\delta] + F[\infty]$, respectively (by hypothesis, $F_-[\infty] = F_+[\infty] = F[\infty]$). Since the decision in both models is based upon the absolute value of the chromatic response $y(t)$, $F_-[\delta] = -F_+[\delta]$, and the heterochromatic–homochromatic difference $F_-[\delta] + F[\infty] - F_+[\delta] - F[\infty] = 2F[\delta]$.

When $|a_0| \ll |a_1|$, $F[\delta]$ approximates the shape of $h(t)$ if peak detection occurs (Roufs & Blommaert, 1981). Thus if the peak detection model is correct, Fig. 8 may provide a good approximation to the actual impulse response. This is not true for probability summation, however (Watson, 1982), nor is it true for Fig. 9 even if peak detection is correct since $|a_0| = |a_1|$.

When the two pulses are identical ($a_0 = a_1$), then $y_\delta(t) = y_{-\delta}(t)$, and it does not matter which pulse is first. When $a_0 = -a_1$, $y_\delta(t) = -y_{-\delta}(t)$, since there is linearity up to the decision stage and we assume that detection is independent of polarity. Thus, when $|a_0| = |a_1|$, the threshold vs ISI function $F[\delta]$ must be even-symmetric about zero ISI, for both detection models. The interaction between the two pulses will be maximal at $\delta = 0$. Therefore when the pulse amplitudes are equal, the two-pulse method cannot reveal the presence of an absolute delay, or the rising portion of the IRF.

When the two pulse magnitudes are not equal, the largest interaction is still at zero ISI, but an asymmetry in $F[\delta]$ could in principle provide information about the rising portion of the IRF. Such as asymmetry could arise under either model, but any deviation from symmetry is likely to be small. In the present experiments, we only measured the right-hand side of $F[\delta]$ (the larger pulse came later), and therefore we could not expect to see any effect of the rising portion of the IRF in our data: the rising portion must be inferred from the model.

Peak detector and probability summation model fits

The peak detector model parameters were estimated by minimizing the sum, over δ, of $[\max\{|y_\delta(t)|\} - 1]^2$, using Powell's method (Press, Flannery, Teukolsky & Vetterling, 1986). The experiments in which the total observation interval was kept constant (Figs 7 and 9) were weighted double in the fit, but all data were weighted equally in calculating the residual mean square error (this is a conservative calculation of error).

In addition to fitting the peak detector model, some trial calculations were made with the probability summation model. This model can be applied in a straightforward way when the two pulses are varied together (Fig. 9). The following approach was used when the first pulse was fixed (Figs 6 and 7).

For measured detection rates we assume a 50% guess probability. For a single pulse,

$$P(a) = 1 - \tfrac{1}{2}\exp\left[-\int_0^\infty |a \cdot h(t)|^{\gamma_1} \, dt\right]. \tag{A3}$$

Similarly, for a presentation of two pulses,

$$P_\delta(a_1|a_0) = 1 - \left[1 - \frac{1}{2}\right] \cdot \exp\left[-\int_0^{\gamma_2} |a_0 \cdot h(t) + a_1 \cdot h(t-\delta)|^{\gamma_2} \, dt\right]. \tag{A4}$$

Equations (A3) and (A4) are theoretical assertions based upon Watson's (1979) model of probability summation. We next set equation (A4) equal to equation (3) and find

$$1 - [1 - P(a_0)] \cdot \exp[-(a_1/\hat{a}_\delta)^{\beta_\delta}]$$

$$= 1 - \left[1 - \frac{1}{2}\right] \cdot \exp\left[-\int_0^\infty |a_0 \cdot h(t) + a_1 \cdot h(t-\delta)|^{\gamma_2}\, dt\right].$$

Substituting equation (A3) for $P(a_0)$ on the left side and performing simple algebra yields

$$\int_0^\infty |a_0 \cdot h(t)|^{\gamma_1}\, dt + [a_1/\hat{a}_\delta]^{\beta_\delta} = \int_0^\infty |a_0 \cdot h(t) + a_1 \cdot h(t-\delta)|^{\gamma_2}\, dt. \quad \text{(A5)}$$

Equation (A5) is exact; however, in the fits we assumed that $\gamma_1 \cong \gamma_2 \cong \beta_\delta = \beta$—the average of the measured psychometric slopes, making the analysis approximate. At threshold, $a_1 = \hat{a}_\delta$ by definition. Impulse-response functions $h(t)$ were fit to the data in Figs 6 and 7 by minimizing the squared-deviation between the two sides of the following equation:

$$\int_0^\infty |a_0 \cdot h(t)|^{\beta}\, dt + 1 = \int_0^\infty |a_0 \cdot h(t) + \hat{a}_\delta \cdot h(t-\delta)|^{\beta}\, dt. \quad \text{(A6)}$$

The error surface defined by the square of equation (A6) had many more local minima and higher residuals than the corresponding surface defined by the peak detector. The best-fitting IRFs were similar to those in Fig. 10 but had later zero crossings and deeper negative lobes, especially for observer CFS.